**The EMBO Journal (2012) 31,** 945–958 | © 2012 European Molecular Biology Organization | All Rights Reserved 0261-4189/12
www.embojournal.org

THE EMBO JOURNAL

# VprBP binds full-length RAG1 and is required for B-cell development and V(D)J recombination fidelity

**Michele D Kassmeier[1,4], Koushik Mondal[1,4], Victoria L Palmer[1,4], Prafulla Raval[1,4,5], Sushil Kumar[1,6], Greg A Perry[1], Dirk K Anderson[1,7], Pawel Ciborowski[2], Sarah Jackson[3], Yue Xiong[3] and Patrick C Swanson[1,*]**

[1]Department of Medical Microbiology and Immunology, Creighton University Medical Center, Omaha, NE, USA, [2]Department of Pharmacology and Experimental Neuroscience, University of Nebraska Medical Center, Omaha, NE, USA and [3]Department of Biochemistry and Biophysics, Lineberger Comprehensive Cancer Center, University of North Carolina Medical Center, Chapel Hill, NC, USA

**The N-terminus of full-length RAG1, though dispensable for RAG1/2 cleavage activity, is required for efficient V(D)J recombination. This region supports RING E3 ubiquitin ligase activity *in vitro*, but whether full-length RAG1 functions as a single subunit or a multi-subunit E3 ligase *in vivo* is unclear. We show the multi-subunit cullin RING E3 ligase complex VprBP/DDB1/Cul4A/Roc1 associates with full-length RAG1 through VprBP. This complex is assembled into RAG protein–DNA complexes, and supports *in-vitro* ubiquitylation activity that is insensitive to RAG1 RING domain mutations. Conditional B lineage-specific *VprBP* disruption arrests B-cell development at the pro-B-to-pre-B cell transition, but this block is bypassed by expressing rearranged immunoglobulin transgenes. Mice with a conditional *VprBP* disruption show modest reduction of D–$J_H$ rearrangement, whereas $V_H$–$DJ_H$ and $V_\kappa$–$J_\kappa$ rearrangements are severely impaired. D–$J_H$ coding joints from *VprBP*-insufficent mice show longer junctional nucleotide insertions and a higher mutation frequency in D and J segments than normal. These data suggest full-length RAG1 recruits a cullin RING E3 ligase complex to ubiquitylate an unknown protein(s) to limit error-prone repair during V(D)J recombination.**

*The EMBO Journal* (2012) **31,** 945–958. doi:10.1038/emboj.2011.455; Published online 13 December 2011
*Subject Categories*: immunology
*Keywords*: DDB1; E3 ubiquitin ligase; RAG1; V(D)J recombination; VprBP

*Corresponding author. Department of Medical Microbiology and Immunology, Creighton University Medical Center, 2500 California Plaza, Omaha, NE 68178, USA. Tel.: +1 402 280 2716; Fax: +1 402 280 1875; E-mail: pswanson@creighton.edu
[4]These authors contributed equally to this work
[5]Present address: Department of Chemistry, Creighton University, Omaha, NE 68178, USA
[6]Present address: Department of Biochemistry and Molecular Biology, University of Nebraska Medical Center, Omaha, NE 68198, USA
[7]Present address: Accuri Cytometers 173 Parkland Plaza, Ann Arbor, MI 48103, USA

**Received: 24 June 2011; accepted: 11 November 2011; published online: 13 December 2011**

## Introduction

B and T lymphocytes have the unique capacity for antigen-specific recognition, which is mediated by immunoglobulins (Igs) and T-cell receptors (TCRs), respectively. The exons encoding the antigen-binding domains of Igs and TCRs must be assembled from variable (V), joining (J) and sometimes diversity (D) gene segments to gain functionality, which is achieved through a site-specific DNA rearrangement process called V(D)J recombination. V(D)J recombination is understood to occur in two distinct phases: the 'cleavage phase' and the 'joining phase' (Fugmann *et al*, 2000; Gellert, 2002). In the cleavage phase, two different gene segments are brought into close proximity by two lymphoid cell-specific proteins, called RAG1 and RAG2, which bind a conserved sequence element flanking each gene segment, called the recombination signal sequence (RSS). The RAG proteins then introduce a DNA double-strand break (DSB) coordinately at the 5′ end of each RSS, liberating two blunt signal ends, and two coding ends terminating in covalently sealed DNA hairpin structures. After cleavage, the DSBs are subsequently transitioned into the joining phase, during which the DNA ends are reorganized, processed and joined by components of the non-homologous end joining (NHEJ) repair pathway (Lieber, 2010). Typically as a result, the two gene segments become joined to one another to form a 'coding joint' that is often imprecise, and the two RSSs become precisely joined to create a 'signal joint'.

RAG protein structure–function analysis reveals that RAG1 can support V(D)J recombination of extrachromosomal and integrated substrates even when ~1/3rd of the protein is removed from the N-terminus (residues 1–383 of 1040 amino acids) (Sadofsky *et al*, 1993; Silver *et al*, 1993; Kirch *et al*, 1996). Although dispensable for the basic catalytic activity of the recombinase, the N-terminus of RAG1 is evolutionarily conserved (Sadofsky *et al*, 1993), and is necessary to support rearrangement of endogenous loci with high efficiency and fidelity (Dudley *et al*, 2003; Talukder *et al*, 2004). The RAG1 N-terminus was recognized to contain a $C_3HC_4$ RING finger domain (Yurchenko *et al*, 2003), a motif commonly found in members of a large family of E3 ubiquitin (Ub) ligases that catalyse Ub transfer in the Ub modification system (Deshaies and Joazeiro, 2009). In this system, Ub is used to modify intracellular proteins to regulate their stability or function as a mechanism to control cellular responses. This process is achieved through three steps: (i) ATP-dependent loading of Ub to an Ub-activating enzyme (E1); (ii) transfer of Ub from the E1 enzyme to a Ub-conjugating enzyme (E2) and (iii) transfer of Ub from the E2–Ub complex to a lysine residue of a substrate protein catalysed by an E3 Ub ligase. Given the presence of a RING finger domain in the RAG1 N-terminus, this region was speculated to regulate V(D)J recombination by functioning as an E3 Ub ligase to target itself or other proteins. In support of this possibility, two studies showed that an isolated RAG1 N-terminal fragment containing the RING domain supports auto-ubiquitylation

©2012 European Molecular Biology Organization

(Jones and Gellert, 2003), and ubiquitylation of a test substrate *in vitro* (Yurchenko *et al*, 2003). Subsequent studies revealed that RAG1 can promote ubiquitylation of two different N-terminal RAG1-interacting proteins, KPNA1 (Simkus *et al*, 2009) and histone H3 (Grazini *et al*, 2010), and perhaps more specifically the acetylated form of histone H3.3 (Jones *et al*, 2011). The functional relevance of RAG1-mediated ubiquitylation of these substrates remains obscure. It is notable in this regard that both of these RAG1-interacting proteins were initially identified in assays using RAG1 only in the absence of RAG2 (Cortes *et al*, 1994; Grazini *et al*, 2010). Whether RAG1 interactions with RAG2 or other factors alter the spectrum of targets ubiquitylated by RAG1 is unclear. Moreover, since many RING-type E3 Ub ligases consist of multi-subunit assemblies containing various adaptor and substrate receptor proteins (Deshaies and Joazeiro, 2009), whether RAG1 functions physiologically as an E3 Ub ligase independent of accessory proteins, or whether such factors are required for its ubiquitylation activity towards physiological substrates remains to be clarified. Here, we show that components of a cullin E3 Ub ligase complex that includes the scaffold protein Cul4A and its associated RING finger domain protein Roc1 (also called Rbx1), the adaptor protein *d*amaged *D*NA *b*inding protein 1 (DDB1), and the substrate receptor protein *Vpr b*inding *p*rotein (VprBP; also called DCAF1) are all co-purified with full-length RAG1, and that VprBP is required for B-cell development and high-fidelity V(D)J recombination.

## Results

### *A complex containing VprBP, DDB1, Cul4A and Roc1 interacts with full-length RAG1*

We previously showed that co-expressed N-terminal maltose binding protein (MBP)-tagged full-length RAG1 and core RAG2 purified under mild conditions (FLMR1/cMR2) support formation of a RAG–RSS complex containing two NHEJ factors, Ku70 and Ku80, detectable by electrophoretic mobility shift assay (EMSA) (this complex is called RAG/Ku–RSS) (Raval *et al*, 2008). In these experiments, Ku70/Ku80 failed to supershift a lower order RAG–RSS complex assembled with FLMR1/cMR2, suggesting an unidentified bridging molecule or cofactor mediates the RAG–Ku interaction (Raval *et al*, 2008). In support of this hypothesis, FLMR1/cMR2 preparations routinely showed two additional protein bands on SDS–PAGE gels, called p120 and p170, which were absent in RAG preparations containing core RAG1 and either core or full-length RAG2 (Figure 1A). Using mass spectrometry, p170 was identified as VprBP (also called DCAF1) (Figure 1B). VprBP is a member of the WD40-repeat family of proteins (Lee and Zhou, 2007), and reportedly functions as a substrate receptor in at least two different E3 Ub ligase complexes in non-lymphoid cells: the RING-type DDB1/Cul4A/Roc1 complex (Huang and Chen, 2008) and the HECT-type DDB1/DYRK2/EDD complex (Maddika and Chen, 2009). Because DDB1 is a 127-kDa protein that co-purifies with VprBP in nearly equivalent amounts (Wen *et al*, 2007), we speculated that p120 was DDB1. Immunoblotting confirmed the presence of VprBP, DDB1 and Cul4A and Roc1 (weakly) in preparations of FLMR1/cMR2, but not cMR1/cMR2 and cMR1/FLMR2 (Figure 1C). DYRK2 and EDD were not detected in purified FLMR1/cMR2 preparations (Supplementary Figure S1A), suggesting they are not stably integrated into an E3 Ub ligase complex containing full-length RAG1.

### *VprBP/DDB1 associates with FLMR1/cMR2 and Ku in a higher order protein–DNA complex*

Having established that VprBP, DDB1, Cul4A and Roc1 (hereafter termed the VDCR complex) co-purify with FLMR1/cMR2, we asked whether any of these components are present in the higher order RAG/Ku–RSS complex that is detected in binding reactions containing FLMR1/cMR2 but not cMR1/cMR2 (Figure 1D, compare lanes 1 and 4). We focused on VprBP because of its putative role as substrate receptor for E3 Ub ligases. We found that anti-VprBP antiserum, but not pre-immune serum, specifically depleted the RAG/Ku–RSS complex, but not the lower order RAG–RSS complex in the same lane (Figure 1D, compare lanes 5 and 6). In addition, VprBP/DDB1 purified from insect cells with or without Cul4A and Roc1 did not supershift RAG–RSS complexes assembled with cMR1/cMR2, but stimulated formation of the higher order RAG/Ku–RSS complex in samples containing FLMR1/cMR2 (Figure 1E, compare lane 4 with lanes 5 and 6, and lane 7 with lanes 8 and 9). This result suggests VprBP/DDB1 is stably integrated into the RAG/Ku–RSS complex. Consistent with this notion, VprBP-specific antibody supershifted the RAG/Ku–RSS complex in all samples containing FLMR1/cMR2 regardless of whether Cul4A/Roc1 was present (Figure 1E, compare lanes 7–9 with 10–12). These data suggest Cul4A and Roc1 are dispensable for stable association of VprBP/DDB1 with the RAG/Ku–RSS complex.

### *RAG1 interactions with VprBP are primarily mediated by the WD40 motif of VprBP and the far N-terminus of full-length RAG1*

Because VprBP functions as a substrate receptor for other E3 Ub ligases, we suspected that VprBP directly interacts with FLMR1/cMR2. To test this possibility, we incubated purified FLMR1/cMR2 with purified full-length human VprBP (FL), an N-terminal truncation mutant lacking the C-terminal WD40 repeats and acidic tail (D1), or truncation mutants containing only the WD40 repeats (D5), or the acidic tail (D8) (Figure 2A), and then immunoprecipitated the RAG proteins and probed for VprBP by immunoblotting. We found that both full-length VprBP and the D5 fragment readily co-immunoprecipitated (co-IP) with the RAG proteins, but the D1 and D8 fragments did so poorly (D1) or not at all (D8) (Figure 2B). Interestingly, in samples containing full-length VprBP, a contaminating N-terminal VprBP fragment is recovered after IP. This fragment is present in the input and is smaller than the D1 fragment, yet D1 itself associates only weakly with FLMR1/cMR2 (Figure 2B). This outcome is most easily explained if full-length VprBP not only interacts with FLMR1/cMR2 through its WD40 motif, but also associates directly or indirectly with the truncated VprBP fragment. This interaction is most likely indirect, because the LisH motif, which reportedly mediates VprBP oligomerization (Ahn *et al*, 2011), should not be present in the truncated fragment based on its apparent molecular mass (Figure 2B). Alternatively, full-length VprBP may associate with the truncated VprBP fragment through DDB1, because DDB1 co-purifies with both full-length VprBP and the D1 fragment (Supplementary Figure S1A and B). Notably, these experiments rule out the possibility that the RAG proteins directly interact with DDB1,

 ©2012 European Molecular Biology Organization

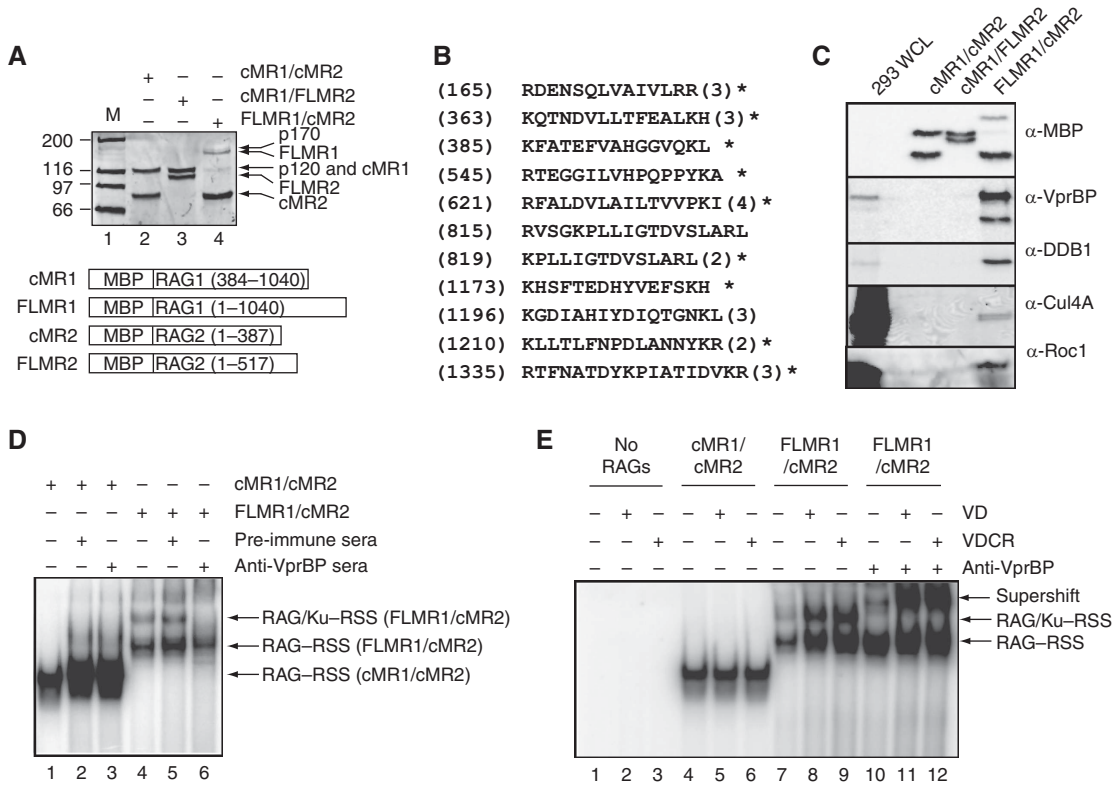


**Figure 1** VprBP and DDB1 associate with full-length RAG1 and core RAG2 and assemble a higher order RAG–RSS complex. (**A**) SYPRO orange-stained SDS–PAGE gels of core and full-length RAG1 and RAG2 preparations purified from HEK293 cells revealed two co-purifying proteins, p120 and p170, in the FLMR1/cMR2 preparation (arrows). Consistent with previous results (Raval *et al*, 2008), the expression and recovery of full-length RAG1 are slightly lower than for core RAG1. Protein standards to determine apparent molecular weight (M) were run in lane 1. Forms of maltose binding protein (MBP)-tagged RAG1 and RAG2 are designated below the gel. (**B**) Peptide sequences identified by mass spectroscopy of trypsin-digested p170. The position of the peptides in the VprBP sequence, the number of times they are represented in the sample, and their presence in multiple, independent samples are indicated in brackets, parentheses, and by an asterisk, respectively. (**C**) Immunoblots of RAG protein preparations in (**A**) using antibodies against MBP, VprBP, DDB1, Cul4A and Roc1, as indicated at right. A sample of whole cell lysate prepared from HEK293 cells (293 WCL) was run along with the RAG protein preparations as a positive control. By SDS–PAGE, all four full-length RAG1-associated proteins migrated to positions consistent with their predicted molecular weight (VprBP, 169 kDa; DDB1, 127 kDa; Cul4A, 80 and 82 kDa; and Roc1, 12 kDa). (**D**) cMR1/cMR2 or FLMR1/cMR2 was incubated with a radiolabelled 12-RSS in the absence or presence of pre-immune or anti-VprBP anti-serum (Zhang *et al*, 2001), and RAG–RSS complex formation visualized by EMSA. (**E**) cMR1/cMR2 or FLMR1/cMR2 binding to a 12-RSS was analysed by EMSA in the absence or presence of purified VprBP/DDB1 and VprBP/DDB1/Cul4A/Roc1 (expressed in insect cells; VD and VDCR, respectively) and with or without subsequent addition of anti-VprBP antibody as indicated. Figure source data can be found in Supplementary data.

because the D1 but not D5 preparation was found to contain DDB1 (Supplementary Figure S2A and B), yet D5 readily bound to FLMR1/cMR2, but D1 did so poorly (Figure 2B).

To further narrow the region within the RAG1 N-terminus required for VprBP association, we probed a previously prepared panel of N-terminal MBP–RAG1 truncation mutants (Raval *et al*, 2008) (co-purified with cMR2 and normalized for RAG1 levels) for the presence of endogenous VprBP (Figure 2C). We found that VprBP levels are substantially reduced when the first 150 residues of RAG1 are removed; truncation of an additional 60 residues largely abolishes VprBP association (Figure 2C). Thus, VprBP primarily interacts with the first 150 residues of RAG1. We also probed an individually expressed and purified form of MBP–RAG1 containing only the N-terminal region (residues 1–383; called $MR1_{1-383}$) and found that this region was sufficient to mediate the association with VprBP (Figure 2C). Immunoblotting also confirmed the presence of DDB1, Cul4A and Roc1 in this preparation (unpublished observations).

### *FLMR1/cMR2 supports RAG1 RING-independent E3 Ub ligase activity in vitro*

An isolated RAG1 N-terminal fragment containing the RING domain has been reported to undergo auto-ubiquitylation and mediate ubiquitylation of KPNA1 *in vitro* (Simkus *et al*, 2009). Histone H3 was subsequently identified as a putative target of RAG1-mediated ubiquitylation (Grazini *et al*, 2010), with the acetylated form of the histone variant H3.3 possibly a more specific target (Jones *et al*, 2011). In addition, both RAG2 and Ku70 are reported targets for ubiquitylation by other Ub ligases (Mizuta *et al*, 2002; Jiang *et al*, 2005; Gama *et al*, 2006). To determine whether one or more of these proteins are ubiquitylated by FLMR1/cMR2, we established an *in-vitro* ubiquitylation reaction using conditions similar to those reported by others (Jones and Gellert, 2003; Yurchenko *et al*, 2003; Simkus *et al*, 2009). Because Ub ligase activity is influenced by the choice of E2 Ub-conjugating enzyme used in the reaction, we first tested a panel of E2 enzymes, chosen based on these previous studies, for their ability to promote FLMR1/cMR2 ubiquitylation activity *in vitro*. We found that

©2012 European Molecular Biology Organization

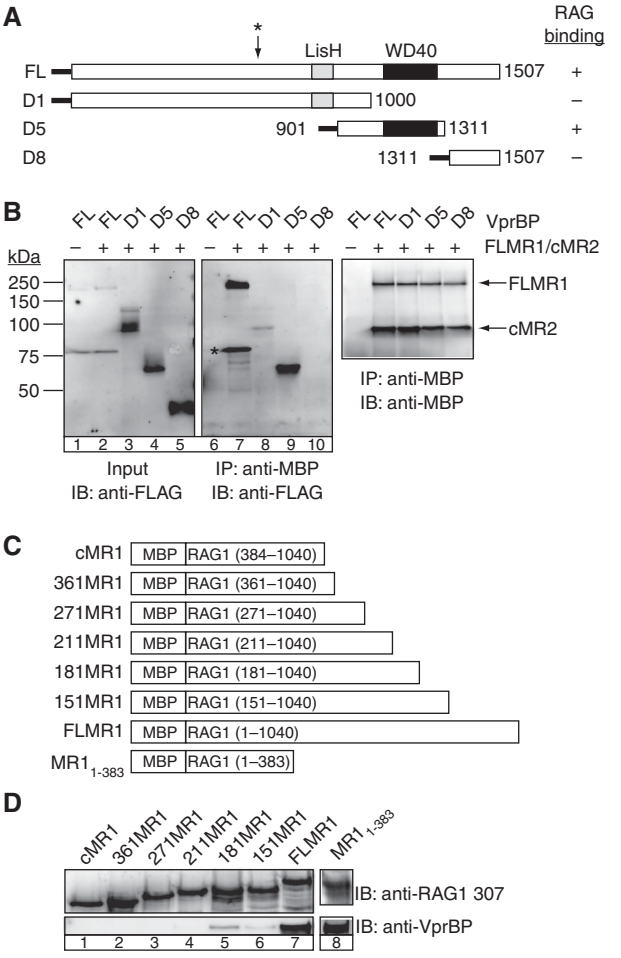


**Figure 2** Full-length RAG1 primarily interacts with the WD40 motif of VprBP. (**A**) Diagram of full-length and truncated forms of VprBP used in this study. A summary of VprBP binding activity from (**B**) is shown at right. The location of a proteolytic site in full-length VprBP is indicated by an asterisk. (**B**) Full-length or truncated VprBP fragments in (**A**) were incubated with purified FLMR1/cMR2 *in vitro* and VprBP binding was assessed by immunoprecipitation (IP) using anti-MBP antibodies followed by immunoblotting (IB) with the indicated antibodies; 5% of the binding reaction was probed directly as a control (input). Note that a proteolytic VprBP fragment present in the input full-length VprBP preparation (indicated by an asterisk) is also recovered after IP (see text for details). (**C**, **D**) Preparations of MBP-tagged RAG1 truncation mutants co-purified with cMR2 described previously (Raval *et al*, 2008) were normalized for RAG1 and analysed by IB to detect RAG1 and VprBP. An individually expressed and purified form of MBP–RAG1 containing only the N-terminal region ($MR1_{1–383}$) was similarly analysed.

purified FLMR1/cMR2, but not cMR1/cMR2, supported robust E2-dependent *de-novo* ubiquitylation *in vitro* in the presence of the E2 enzymes UbcH5a and H5b, but not the other E2 enzymes tested (Figure 3A, top). When these blots were reprobed using MBP-specific antibodies (to detect the RAG proteins), no evidence of *de-novo* ubiquitylation was detected, suggesting that neither RAG1 nor RAG2 is efficient target of RAG1-mediated (auto)ubiquitylation under these conditions (Figure 3A, bottom).

To determine whether ubiquitylation was mediated directly by RAG1, we tested whether an RAG1 RING domain mutation (hC328Y) associated with human Omenn's syndrome (Villa *et al*, 2001) impaired Ub conjugation in our *in-vitro* system. Previous studies have shown that, compared with wild-type (WT) RAG1, a murine equivalent of the human mutant, mC325Y RAG1, exhibits defects in protein folding and reduced activity in assays of auto-ubiquitylation and V(D)J recombination (Simkus *et al*, 2007). For these studies, we prepared not only the mC325Y RAG1 mutant, but also generated an mC328Y RAG1 mutant, because this cysteine residue also participates in zinc ion coordination (Rodgers *et al*, 1996). Consistent with previous results, we found that both RAG1 RING domain mutants showed evidence of protein misfolding as indicated by an increase in endogenous proteolysis and an associated reduction in protein recovery after purification (Supplementary Figure S3A), as well as severely impaired V(D)J recombination activity in assays of signal and coding joint formation (Supplementary Figure S3C and D). Interestingly, both RAG1 mutants supported *in-vitro* ubiquitylation at levels comparable to WT FLMR1/cMR2, suggesting that full-length RAG1 does not directly mediate ubiquitylation in this system (Figure 3B), and raises the possibility that the VDCR complex instead mediates ubiquitylation. In support of this hypothesis, both purified VprBP/DDB1 and Cul4A/DDB1 supported *in-vitro* ubiquitylation in the presence of UbcH5b, but adding FLMR1/cMR2 slightly stimulates this activity *in vitro* (Figure 3C). To determine whether ubiquitylation activity in this experimental system is RAG2 dependent, or dependent on the core region of RAG1, we tested whether purified FLMR1 alone or $MR1_{1–383}$ mediated ubiquitylation *in vitro*. We found that, like FLMR1/cMR2, both FLMR1 alone and $MR1_{1–383}$ supported a similar pattern of E2-dependent ubiquitylation in the presence of UbcH5a and UbcH5b (Figure 3D and E), suggesting that neither RAG2 nor the core portion of RAG1 is required for ubiquitylation activity in this system. Interestingly, when FLMR1 and FLMR1/cMR2 preparations were directly compared in this assay (Figure 3F), FLMR1 showed higher levels of ubiquitylation, suggesting RAG2 may partially inhibit full-length RAG1 ubiquitylation activity *in vitro*.

The failure of RAG1 RING domain mutations to impair *in-vitro* ubiquitylation activity suggests that such mutations disrupt V(D)J recombination by an alternative mechanism. Consistent with this possibility, we found that the RAG1 RING domain mutants exhibit a defect at the cleavage step of V(D)J recombination, as both the mC325Y and mC328Y FLMR1/cMR2 preparations supported lower levels of signal end break (SEB) formation in cells compared with WT FLMR1/cMR2 as detected by ligation-mediated PCR (LM-PCR; Supplementary Figure S3E and F). We attribute the poor cleavage activity of the mutants to a DNA binding defect, because neither the mC235Y or mC328Y FLMR1/cMR2 preparation supported detectable RAG–RSS complex formation by EMSA (Supplementary Figure S3B).

Since KPNA1 and histone H3 have been reported to associate with and be ubiquitylated by RAG1 (Simkus *et al*, 2009; Grazini *et al*, 2010), we tested whether either protein was present in purified FLMR1/cMR2, and indeed detected both proteins by immunoblotting (Supplementary Figure S1B). However, *in-vitro* ubiquitylation experiments failed to provide convincing evidence that KPNA1 or histone H3 (variant H3.1, 3.2 or 3.3) undergoes full-length RAG1-dependent ubiquitylation, either in reactions supplemented with recombinant substrates (Supplementary Figure S4A–C), or in

 ©2012 European Molecular Biology Organization

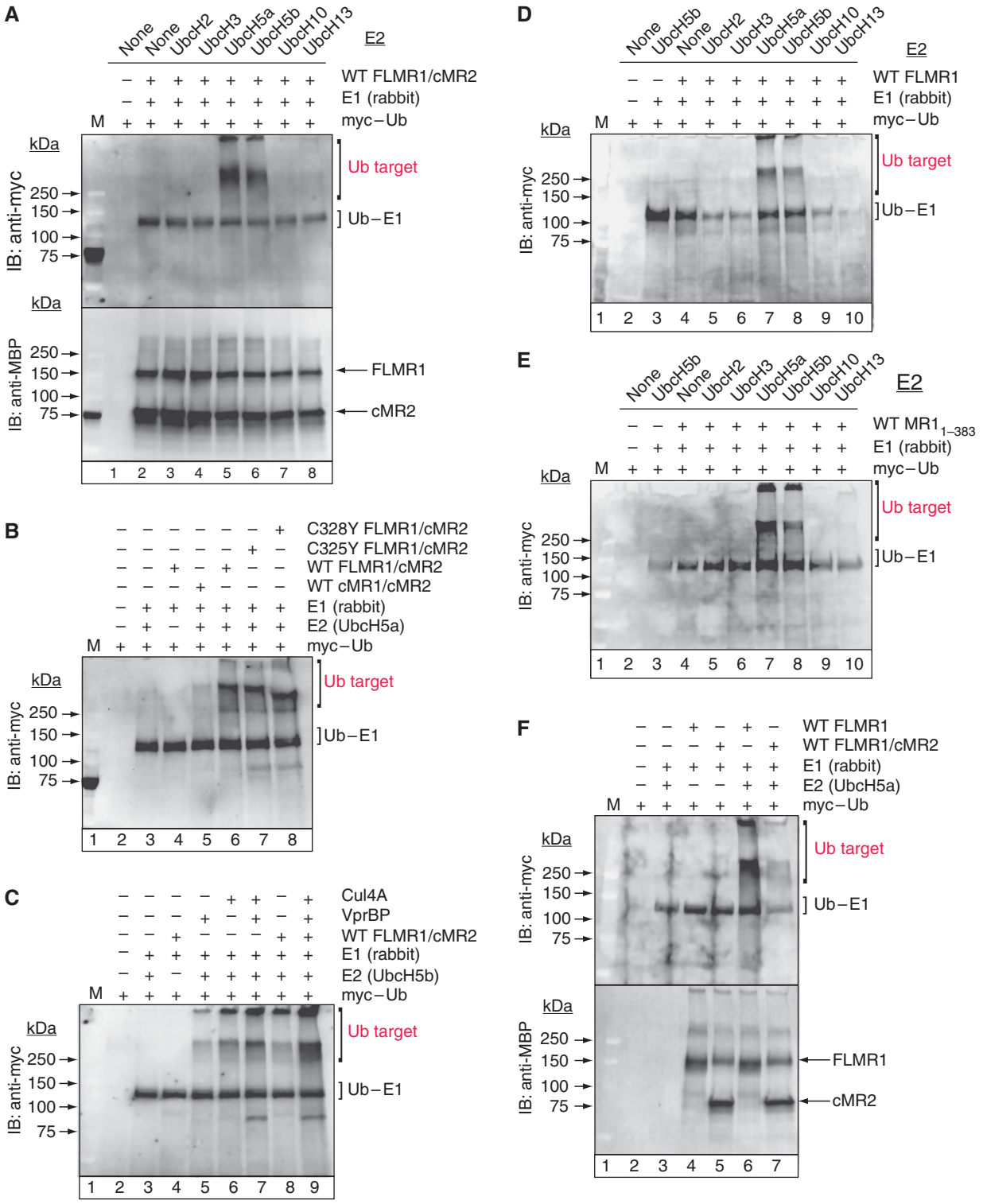


**Figure 3** Purified FLMR1/cMR2 supports RING-independent ubiquitylation of an unknown target protein, but does not undergo efficient auto-ubiquitylation *in vitro*. (**A**) *In-vitro* ubiquitylation reactions containing wild-type (WT) FLMR1/cMR2, myc–Ub, E1 and various E2 carrier proteins were assembled as indicated, incubated as described in Materials and methods, and probed by IB using the antibodies at left. (**B**) *In-vitro* ubiquitylation reactions containing WT, mC325Y, or mC328Y FLMR1/cMR2 preparations were assembled and analysed as in (**A**) using UbcH5a as the E2 carrier. (**C**) *In-vitro* ubiquitylation reactions were assembled as in (**A**) using UbcH5b as the E2 carrier protein, except that some reactions were further supplemented with 293 cell-purified FLAG-tagged VprBP (lanes 5, 7 and 9) and/or Cul4A (lanes 6, 7 and 9). Reactions were analysed as in (**A**). (**D**, **E**) *In-vitro* ubiquitylation reactions were assembled and analysed as in (**A**), except that FLMR1/cMR2 was replaced by individually expressed and purified FLMR1 (**D**) or $MR1_{1–383}$ (**E**). (**F**) *In-vitro* ubiquitylation reactions containing wild-type FLMR1 or FLMR1/cMR2 preparations were assembled and analysed as in (**A**) using UbcH5a as the E2 carrier protein. Figure source data can be found in Supplementary data.

©2012 European Molecular Biology Organization

reactions containing only the endogenous co-purified proteins (unpublished observations). We also performed *in-vitro* ubiquitylation reactions using Ku70 and Ku80 as test substrates based on our previous studies showing that both proteins associate with full-length RAG1 (Raval *et al*, 2008), but these experiments yielded equivocal results as well (Supplementary Figure S4D). Since the evidence suggests that KPNA1, histone H3 and Ku70/80 are not robust ubiquitylation targets in this experimental system, we performed a time-course study to determine whether mono-ubiquitylation of a smaller protein is detectable early in the reaction. However, even at the earliest time points, only high molecular weight ubiquitylated products were detected, which accumulate over time and progress towards higher order polyubiquitylated products that fail to enter the polyacrylamide gel (Supplementary Figure S4E). Taken together, these experiments favour a model in which FLMR1 recruits the VDCR complex to target one or more proteins for ubiquitylation that are distinct from those previously shown to be ubiquitylated by RAG1. However, we cannot formally exclude the possibility that in this experimental system, a small protein in limited abundance is targeted for ubiquitylation, but cannot be readily detected until it becomes polyubiquitylated. Such a possibility would make it difficult to identify the target.

### *Conditional disruption of VprBP expression in the B lineage blocks B-cell development at the pro-B-to-pre-B cell transition by triggering cell-cycle arrest and apoptosis*

If the VDCR complex plays an essential role in V(D)J recombination, disrupting expression of one or more of these components early in lymphocyte development would be expected to arrest maturation at a developmental stage similar to that observed in RAG-deficient mice. In the B lineage, conventional gene-targeted disruption of *RAG1* or *RAG2* arrests maturation at the pro-B-to-pre-B cell transition (Mombaerts *et al*, 1992; Shinkai *et al*, 1992). Because VprBP is a known substrate receptor for E3 Ub ligases (Huang and Chen, 2008; Maddika and Chen, 2009) and directly interacts with RAG1 (Figure 2), we wished to test whether loss of VprBP function impairs lymphocyte development and V(D)J recombination. However, since conventional *VprBP* disruption causes early embryonic lethality (McCall *et al*, 2008), we instead employed a Cre-*loxP* approach to conditionally disrupt *VprBP* expression in the B lineage using mb1-Cre transgenic mice that express Cre from the very early pro-B cell stage onwards ($Cre^+$) (Hobeika *et al*, 2006), and mice bearing a conditional *VprBP* allele in which exons 7 and 8 are flanked by *loxP* sites ($VprBP^{fl}$; see Figure 4A and McCall *et al*, 2008).

Bone marrow, spleens and thymi were collected from 4- to 6-week-old WT, $VprBP^{fl/+}$-$Cre^-$, $VprBP^{fl/fl}$-$Cre^-$, $VprBP^{fl/+}$-$Cre^+$, $VprBP^{fl/fl}$-$Cre^+$ and $RAG1^{-/-}$ mice and B- and T-cell developmental subsets were analysed by flow cytometry (Figure 4B; Supplementary Figure S5). We found that $VprBP^{fl/+}$-$Cre^-$, $VprBP^{fl/fl}$-$Cre^-$ and $VprBP^{fl/+}$-$Cre^+$ mice immunophenotypically resembled each other and WT mice. Strikingly, compared with $VprBP^{fl/+}$-$Cre^+$ mice, $VprBP^{fl/fl}$-$Cre^+$ mice exhibited a profound block at the pro-B-to-pre-B cell transition, as evidenced by a five-fold ($P<0.005$) decrease in bone marrow $B220^+CD43^-$ cells, whereas the frequency of $B220^+CD43^+$ cells was unaffected (Figure 4B, first row; Figure 4C). Within the $B220^+CD43^+$ subset, pre/pro-B cell ($CD19^-CD24^-$) and pro-B cell ($CD19^+CD24^+$) fractions were not significantly different between the genotypes (Supplementary Figure S5A). Consistent with a block in early B-cell development, few if any B cells with an immature ($IgM^+IgD^-$) or mature ($IgM^+IgD^+$) phenotype were detected in bone marrow or spleen of $VprBP^{fl/fl}$-$Cre^+$ mice (Figure 4B, second and third rows; Figure 4C). The B-cell developmental block observed in $VprBP^{fl/fl}$-$Cre^+$ mice is very similar to that reported for $RAG1^{-/-}$ mice and reproduced here (Shinkai *et al*, 1992; Spanopoulou *et al*, 1994; Figure 4B, compare last two columns). As expected from the B-lineage restricted Cre expression in this system, $VprBP^{fl/fl}$-$Cre^+$ mice exhibited no significant differences in the abundance or distribution of T-cell subsets compared with WT, $VprBP^{fl/+}$-$Cre^-$ and $VprBP^{fl/+}$-$Cre^+$ mice (Supplementary Figure S5B), but were distinct from $RAG1^{-/-}$ mice which showed a block in T-cell development at the $CD4^-CD8^-$ stage (Supplementary Figure S5B). Consistent with a profound block in B-cell development, spleen cellularities in $VprBP^{fl/fl}$-$Cre^+$ mice were about 25% lower than in $VprBP^{fl/+}$-$Cre^+$ mice ($6.9 \pm 2.5 \times 10^6$ versus $9.0 \pm 2.1 \times 10^6$, respectively), whereas total bone marrow and thymic cellularities were similar.

To investigate the mechanism of impaired pro-B-to-pre-B cell progression in $VprBP^{fl/fl}$-$Cre^+$ mice, bone marrow $B220^+CD43^+$ and $B220^+CD43^-$ B-cell subsets were sorted from $VprBP^{fl/+}$-$Cre^-$, $VprBP^{fl/+}$-$Cre^+$, $VprBP^{fl/fl}$-$Cre^+$ and $RAG1^{-/-}$ mice and analysed for differences in the frequency of early and late apoptotic cells (defined as staining positive for Annexin V and either negative (early) or positive (late) for propidium iodide, respectively) and cell-cycle status. We found that the percentages of apoptotic cells and cells in the G1, S and G2 phases of the cell cycle among sorted $B220^+CD43^+$ B cells were not significantly different between the various genotypes (Figure 5A). By contrast, relative to $VprBP^{fl/+}$-$Cre^+$ mice, sorted $B220^+CD43^-$ B cells from $VprBP^{fl/fl}$-$Cre^+$ mice showed a significant ~3-fold increase in late apoptotic cells (Annexin $V^+PI^+$) and a similar increase in S phase cells (Figure 5B). These results were similar to those obtained from $RAG1^{-/-}$ mice analysed in parallel (Figure 5B). Taken together, these data suggest that B cells emerging from the $B220^+CD43^+$ cell stage in $VprBP^{fl/fl}$-$Cre^+$ mice enter cell cycle, but fail to transit through S phase, triggering the onset of apoptosis.

### *Enforced Ig transgene expression rescues B-cell development in $VprBP^{fl/fl}$-$Cre^+$ mice*

To exclude the possibility that the block in B-cell development observed in $VprBP^{fl/fl}$-$Cre^+$ mice is independent of V(D)J recombination, we bred functionally rearranged heavy and light chain transgenes specific for hen egg lysozyme (IgHEL) onto the $VprBP^{fl/fl}$-$Cre^+$ strain background. We reasoned that if VprBP is directly involved in V(D)J recombination, IgHEL expression should enable developing B cells to bypass the developmental block imposed by loss of VprBP function, by analogy to comparable experiments performed in $RAG1^{-/-}$ mice (Spanopoulou *et al*, 1994). Consistent with this expectation, flow cytometric analysis of IgHEL-expressing $VprBP^{fl/fl}$-$Cre^+$ mice revealed an increased percentage of $B220^+CD43^-$ B cells in the bone marrow relative to $VprBP^{fl/fl}$-$Cre^+$ mice (Figure 6A, top row;

 ©2012 European Molecular Biology Organization

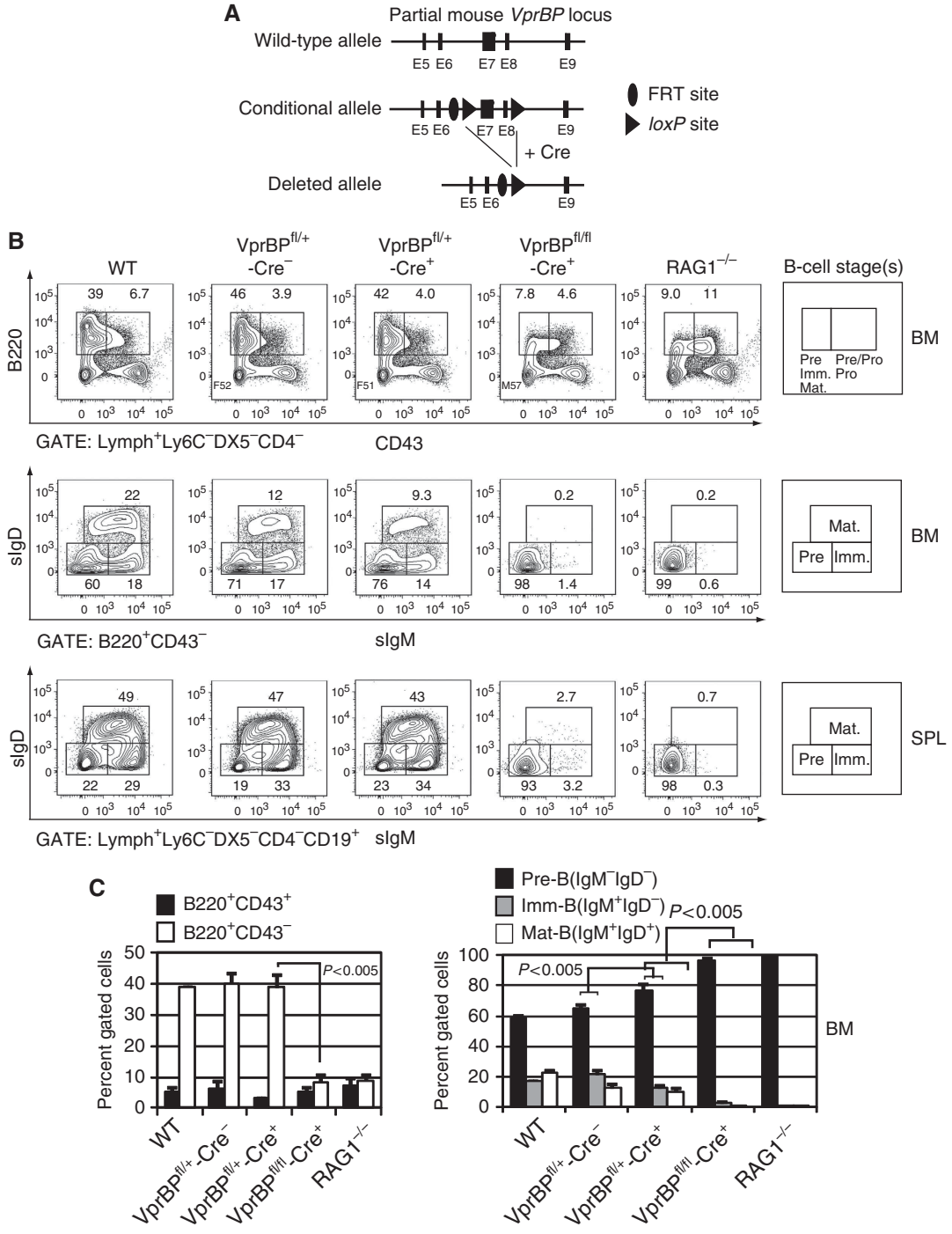


**Figure 4** Conditional disruption of *VprBP* impairs B-cell development. (**A**) Diagram of wild-type, targeted and deleted *VprBP* alleles, adapted from McCall *et al* (2008). (**B**) Flow cytometric analysis of B-cell development. Mice bearing 0, 1 or 2 targeted VprBP alleles (WT, $VprBP^{fl/+}$ or $VprBP^{fl/fl}$, respectively) that do or do not express Cre recombinase in the B lineage ($Cre^+$ or $Cre^-$) as indicated above the panel were analysed for the expression of B220 and CD43 (top row) or sIgM and sIgD (middle and bottom rows) on cells prepared from bone marrow (BM) or spleen (SPL) and identified by the gating parameters shown below each row. Developmental subsets specified by the staining pattern are indicated at right with corresponding gates. The percentage of cells within identified gates or quadrants are shown for representative animals. (**C**) Data collected from 3 to 4 animals of each genotype for the BM samples in (**B**) are summarized in bar graph format. Statistically significant differences determined from analysis of variance and *post hoc* testing using an unpaired *t*-test are indicated. Results obtained from analysis of sIgM and sIgD expression in SPL were comparable to BM.

Figure 6B), and the presence of phenotypically mature B cells in the bone marrow and spleen (Figure 6A, second and third rows; Figure 6B). The frequency of cells comprising the various bone marrow and splenic B-cell subsets was not significantly different between $VprBP^{fl/+}$-$Cre^+$ $IgHEL^+$ and $VprBP^{fl/fl}$-$Cre^+$ $IgHEL^+$ mice (Figure 6B). Splenic $CD19^+$ B cells in $VprBP^{fl/fl}$-$Cre^+$ $IgHEL^+$ mice were also stained by Alexa647-conjugated HEL ($HEL^+$), confirming functional IgHEL transgene expression (Figure 6A, bottom row). This staining is specific because $IgHEL^-$ mice showed no evidence

©2012 European Molecular Biology Organization

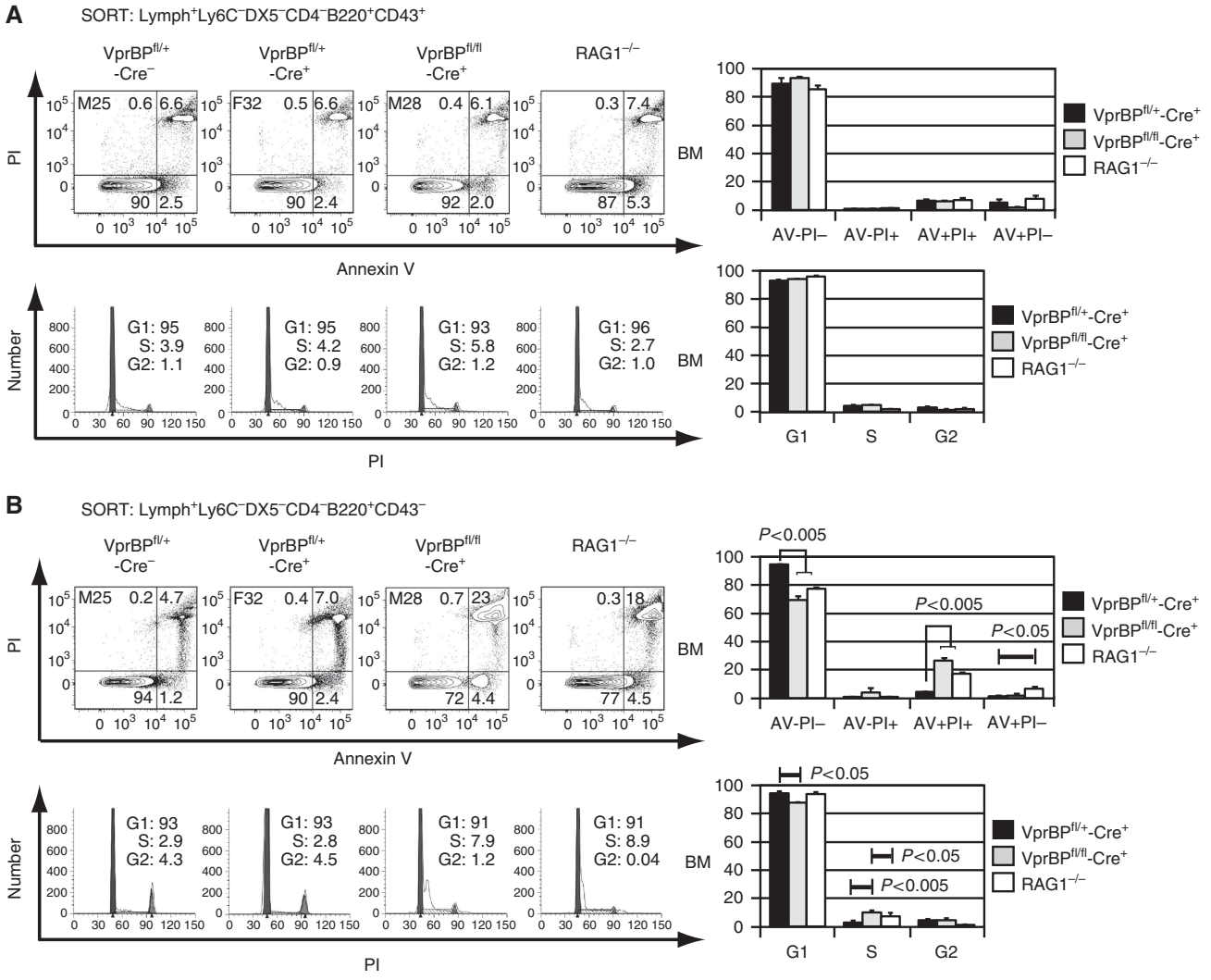


**Figure 5** Developing B cells in VprBP$^{fl/fl}$-Cre$^{+}$ and RAG1$^{-/-}$ mice similarly undergo cell-cycle arrest and apoptosis at the pro-B-to-pre-B cell transition. (**A**) B220$^{+}$CD43$^{+}$ and (**B**) B220$^{+}$CD43$^{-}$ B cells were purified by FACS from bone marrow of VprBP$^{fl/+}$-Cre$^{-}$, VprBP$^{fl/+}$-Cre$^{+}$, VprBP$^{fl/fl}$-Cre$^{+}$ and RAG1$^{-/-}$ mice as indicated above the panels (stained and gated as in Figure 3, top row), and stained with Annexin V and propidium iodide (top row) to analyse the extent of cell apoptosis, or stained with Vindelov's reagent (bottom row) to analyse cell-cycle status. The percentage of cells within each quadrant or cell-cycle phase is shown. Data collected from three independent experiments were analysed and displayed as in Figure 4C.

of CD19$^{+}$HEL$^{+}$ cells. Taken together, these data argue that VprBP is required for B-cell development through a specific role in V(D)J recombination.

### *VprBP$^{fl/fl}$-Cre$^{+}$ mice exhibit impaired $V_H$–$DJ_H$ and $V_\kappa$–$DJ_\kappa$ rearrangements, and loss of VprBP expression is associated with reduced fidelity of V(D)J recombination*

Given the profound block in B-cell development observed in VprBP$^{fl/fl}$-Cre$^{+}$ mice, we wished to determine whether loss of VprBP function in the B-cell lineage impairs the efficiency of V(D)J recombination. Towards this end, genomic DNA prepared from bone marrow of VprBP$^{fl/+}$-Cre$^{-}$, VprBP$^{fl/+}$-Cre$^{+}$, VprBP$^{fl/fl}$-Cre$^{+}$ and control RAG1$^{-/-}$ mice was subjected to PCR and Southern blotting to analyse the status of Ig heavy chain D–$J_H$ and $V_H$–$DJ_H$ rearrangements. We found that the pattern of D–$J_H$ rearrangements in bone marrow was quite similar between VprBP$^{fl/+}$-Cre$^{-}$, VprBP$^{fl/+}$-Cre$^{+}$ and VprBP$^{fl/fl}$-Cre$^{+}$ mice (Figure 7, top panel). However, $V_H$–$DJ_H$ rearrangements were substantially diminished in VprBP$^{fl/fl}$-Cre$^{+}$ mice compared with VprBP$^{fl/+}$-Cre$^{-}$ and VprBP$^{fl/+}$-Cre$^{+}$ mice (Figure 7, middle panel). This was also true for $V_\kappa$–$J_\kappa$ rearrangements, which is consistent with the failure of B cells to progress past the pre-B cell stage of development in VprBP$^{fl/fl}$-Cre$^{+}$ mice (Figure 7, bottom panel). As expected, control RAG1$^{-/-}$ mice showed no evidence of heavy or light chain V(D)J rearrangements.

To more closely examine the fidelity of V(D)J recombination, we amplified D–$J_H$4 coding joints and analysed the nucleotide sequences from ~50 clones obtained from VprBP$^{fl/+}$-Cre$^{-}$, VprBP$^{fl/+}$-Cre$^{+}$ and VprBP$^{fl/fl}$-Cre$^{+}$ mice (Supplementary Figure S6A and B). We found that among sequences with nucleotide (nt) insertions that include both palindromic (P) and non-templated (N) additions, the average insertion length was longer in VprBP$^{fl/+}$-Cre$^{+}$ mice (3.42 ± 0.33 nt) and VprBP$^{fl/fl}$-Cre$^{+}$ mice (3.23 ± 0.40 nt) compared with VprBP$^{fl/+}$-Cre$^{-}$ mice (2.74 ± 0.39 nt), but these differences were not statistically significant (Table I). Similarly, the average length of terminal deletions at

 ©2012 European Molecular Biology Organization

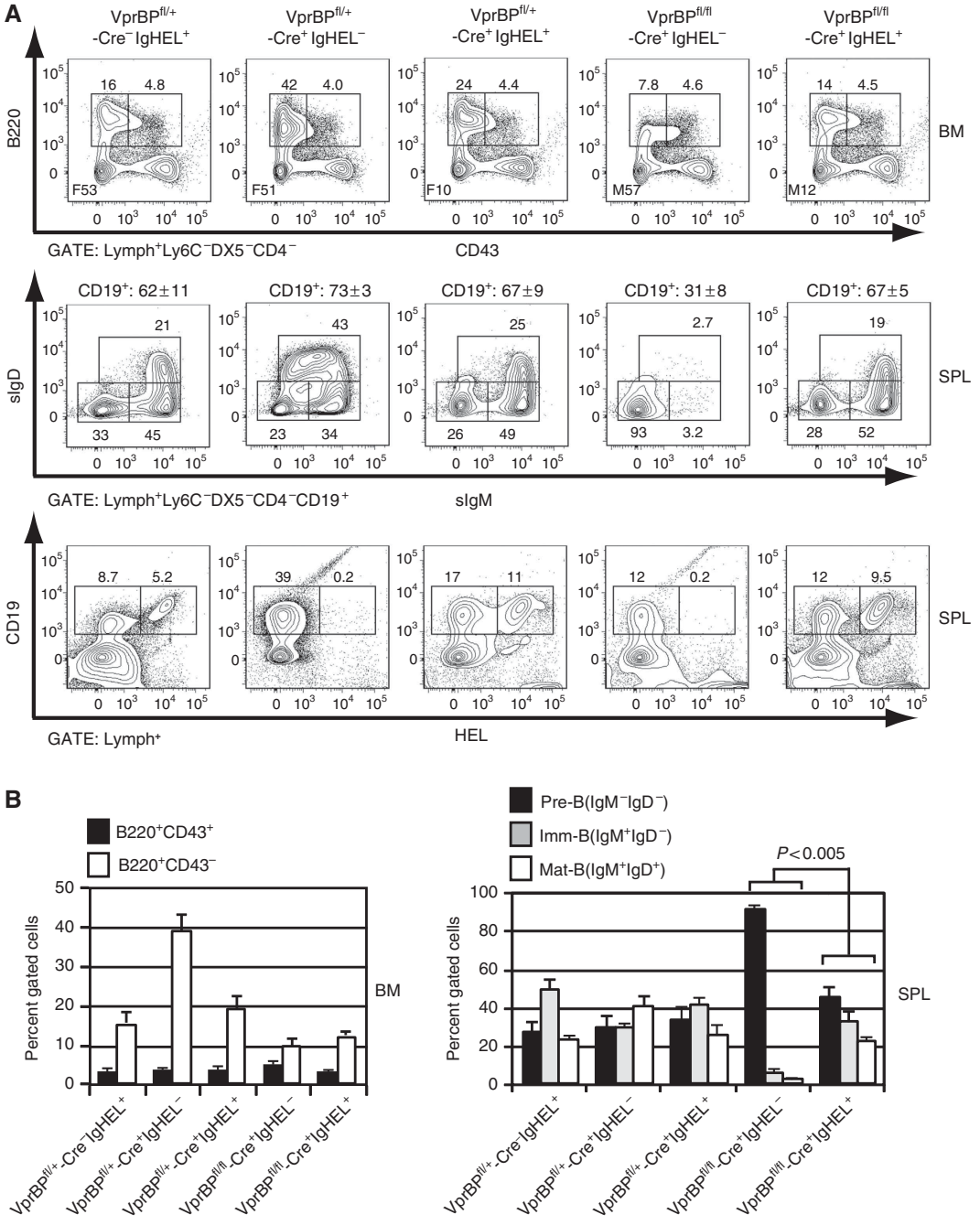


**Figure 6** Expression of functionally rearranged IgHEL transgenes bypasses the developmental block imposed by VprBP deficiency in the B lineage. (**A**) VprBP$^{fl/+}$ or VprBP$^{fl/fl}$ mice expressing Cre and/or IgHEL transgenes as indicated above the panels were analysed for the expression of B220 and CD43 (top row), sIgM and sIgD (second row), and CD19 and HEL (bottom row) on cells prepared from bone marrow (BM) or spleen (SPL) as in Figure 4. (**B**) Data collected from 3 to 4 animals of each genotype for B220 versus CD43 and sIgM versus sIgD expression were analysed and displayed as in Figure 4C.

the $J_H$ segments was longer for VprBP$^{fl/+}$-Cre$^+$ mice (5.75 ± 0.60 nt) and VprBP$^{fl/fl}$-Cre$^+$ mice (4.38 ± 0.64 nt) compared with VprBP$^{fl/+}$-Cre$^-$ mice (4.13 ± 0.44 nt), but these differences were only significant between VprBP$^{fl/+}$-Cre$^+$ mice and VprBP$^{fl/+}$-Cre$^-$ mice (Table I). Interestingly, we also detected an unexpectedly high frequency of small internal insertions, deletions, or mutations in the D and J segments analysed from VprBP$^{fl/+}$-Cre$^+$ mice (4/53 clones) and VprBP$^{fl/fl}$-Cre$^+$ mice (7/47 clones), whereas none were detected in sequences analysed from VprBP$^{fl/+}$-Cre$^-$ mice (Table I; Supplementary Figure S6A–C). In this case, differences between VprBP$^{fl/fl}$-Cre$^+$ mice and VprBP$^{fl/+}$-Cre$^-$ mice were statistically significant. Two features of the mutations are worth noting. First, all mutations identified were transition mutations. Second, all mutations were found in sequences that also had N nucleotide additions or D segment insertions. Finally, we analysed the sequences for evidence of microhomology-directed repair, and identified 5–6 clones from each mouse genotype containing putative microhomology nucleotides (Table I; Supplementary Figure S6A–C).

©2012 European Molecular Biology Organization

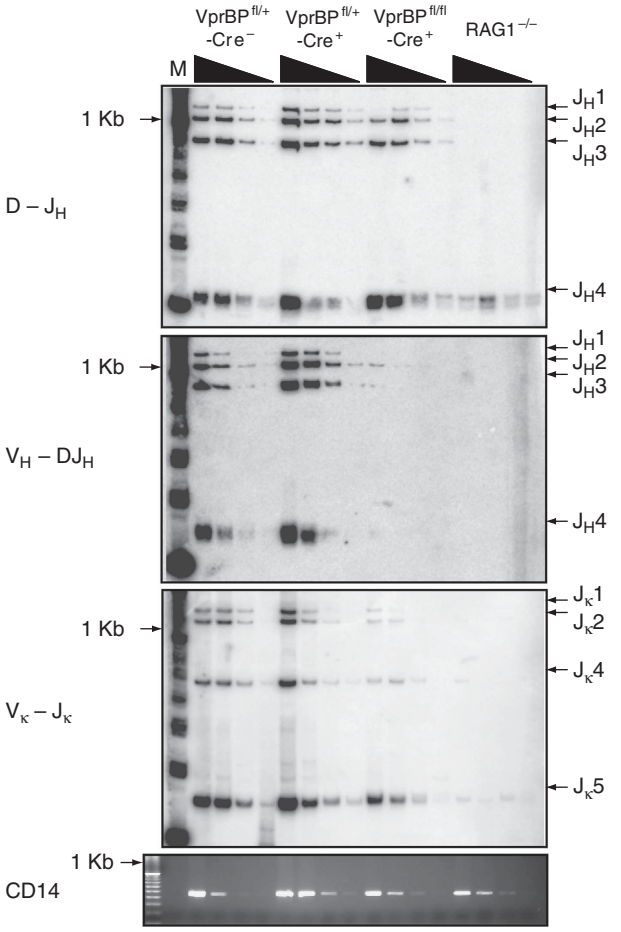


**Figure 7** $V_H$–$DJ_H$ and $V_\kappa$–$J_\kappa$ rearrangements, but not D–$J_H$ rearrangement, are severely impaired in VprBP$^{fl/fl}$-Cre$^+$ mice. Genomic DNA (200–3 ng) isolated from the bone marrow of VprBP$^{fl/+}$-Cre$^-$, VprBP$^{fl/+}$-Cre$^+$, VprBP$^{fl/fl}$-Cre$^+$ and RAG1$^{-/-}$ mice was subjected to PCR–Southern blotting to detect D–$J_H$, $V_H$–$DJ_H$ and $V_\kappa$–$J_\kappa$ gene rearrangements as indicated. PCR amplification of a CD14 gene fragment serves as a loading control in these experiments.

Interestingly, although the frequency of microhomology use is similar, all clones identified from VprBP$^{fl/+}$-Cre$^-$ mice only had short regions of homology ($n = 2$ nt), whereas 3–4 clones identified from VprBP$^{fl/+}$-Cre$^+$ mice and VprBP$^{fl/fl}$-Cre$^+$ mice had longer blocks of homology ($n = 3$–4 nt). Notably, 2/5 clones containing microhomologies identified from VprBP$^{fl/fl}$-Cre$^+$ mice also contained D segment insertions. Taken together, these data suggest that loss of VprBP function reduces the fidelity of DNA end processing and repair events during V(D)J recombination.

## Discussion

### *Full-length RAG1 assembles an E3 Ub ligase complex with E3 ligase adaptor and substrate receptor proteins DDB1 and VprBP*

RING E3 Ub ligases often contain multiple subunits that include a RING domain-containing protein, as well as various adaptor and substrate receptor proteins (Deshaies and Joazeiro, 2009). Although the RAG1 RING finger is known to possess E3 Ub ligase activity *in vitro*, supporting both auto-ubiquitylation (Jones and Gellert, 2003) and ubiquitylation of KPNA1 (Simkus *et al*, 2009) and histone H3 (Grazini *et al*, 2010; Jones *et al*, 2011), it is unclear whether full-length RAG1 functions as a single subunit E3 Ub ligase, or rather associates with other accessory proteins to assemble a multi-subunit E3 Ub ligase complex. The finding here that full-length RAG1 associates with the VprBP/DDB1 complex, which is known to function as an E3 Ub ligase adaptor and substrate receptor complex for both RING-type and HECT-type E3 Ub ligases (Huang and Chen, 2008; Maddika and Chen, 2009; Li *et al*, 2010), favours the latter possibility.

Whether the RAG1 RING domain functions to directly mediate ubiquitylation of protein targets in the context of full-length RAG1 or in the presence of RAG1-interacting factors remains unclear. Using conditions similar to those reported previously, we find that the purified FLMR1/cMR2–VDCR complex does not support RAG1 auto-ubiquitylation, or mediate efficient ubiquitylation of two previously identified targets of *in-vitro* RAG1 E3 Ub ligase activity, KPNA1 or histone H3, or promote ubiquitylation of RAG2 or the Ku proteins. However, the FLMR1/cMR2–VDCR complex does support ubiquitylation of an as-yet unidentified substrate(s) *in vitro* in the presence of UbcH5a or Ubc5b, but this activity is not sensitive to RAG1 C325Y and C328Y RING domain mutations, and occurs independently of RAG2 or the core portion of RAG1. While these results do not preclude the possibility that the RAG1 RING domain functions to directly ubiquitylate protein targets, at the very least our findings indicate that the spectrum of targets potentially ubiquitylated by RAG1 is influenced by factors that associate with full-length RAG1.

Alternatively, because the VDCR complex also co-purifies with the RAG1 RING domain mutants tested in our studies, it is possible that full-length RAG1 does not directly mediate ubiquitylation, but rather recruits another E3 ligase complex to accomplish this task. Indeed, this possibility was raised recently (Jones *et al*, 2011) to explain the apparently modest sensitivity of full-length RAG1-mediated histone H3 ubiquitylation to RAG1 RING domain mutations reported by others (Grazini *et al*, 2010). Our findings are consistent with this possibility, and further suggest that the far N-terminus of RAG1 acts as a scaffold to recruit the VDCR complex to direct its E3 Ub ligase activity. Because the Roc1/Cul4A/DDB1 complex has previously been implicated in mediating ubiquitylation of histones H3 and H4 (Wang *et al*, 2006), our results also provide a plausible alternative mechanism to explain the origin of the ubiquitylated histones detected by Grazini *et al* (2010).

Another interesting finding to emerge from the *in-vitro* ubiquitylation assays is that the FLMR1 alone supports greater ubiquitylation activity than the FLMR1/cMR2 (Figure 3F). Since RAG2 undergoes periodic degradation during the cell cycle (Desiderio, 2010), this observation raises the intriguing possibility that RAG1 ubiquitylation activity (mediated either directly or indirectly by full-length RAG1), is unmasked or upregulated when RAG2 is degraded.

The finding that RAG1 C325Y and C328Y RING mutants characterized here support less RSS cleavage activity than WT RAG1 contrasts with results from a previous study of two similar RAG1 RING mutants (H307A and C325G single or double mutants) that showed SEB accumulation for RAG1 mutants by LM-PCR, but no detectable SEBs for WT RAG1 (Grazini *et al*, 2010). The authors attributed the latter

 ©2012 European Molecular Biology Organization

**Table I** Analysis of D–$J_H$ coding joints

| | VprBP$^{fl/+}$-Cre$^-$ ($n=47$) | VprBP$^{fl/+}$-Cre$^+$ ($n=53$) | VprBP$^{fl/fl}$-Cre$^+$ ($n=47$) |
|---|---|---|---|
| Number repeat | 18/47 | 10/53 | 11/47 |
| *P/N addition* | | | |
| No P/N addition (%) | 11/47 (23.4%) | 9/53 (17.0%) | 13/47 (27.7%) |
| Average P/N length | 2.74 ± 0.39 | 3.42 ± 0.33 | 3.23 ± 0.40 |
| Range | 0–12 | 0–9 | 0–9 |
| *D segment analysis* | | | |
| No deletion (%) | 11/47 (23.4%) | 19/53 (35.8%) | 18/47 (38.3%) |
| Average deletion length | 2.87 ± 0.46 | 2.94 ± 0.53 | 2.45 ± 0.47 |
| Range | 0–15 | 0–20 | 0–18 |
| *JH4 segment analysis* | | | |
| No deletion (%) | 9/47 (19.1%) | 9/53 (17.0%) | 10/47 (21.3%) |
| Average length deletion | 4.13 ± 0.44 | 5.75 ± 0.60[a] ($P=0.044$) | 4.38 ± 0.64 |
| Range | 0–13 | 0–16 | 0–21 |
| *Internal insertion/deletion/substitution*[b] | 0/47 | 4/53 | 7/47[a] ($P=0.006$) |
| Average length I/D/S | 0 | 0.09 ± 0.04 | 0.19 ± 0.08[a] ($P=0.009$) |
| Range | 0 | 0–1 | 0–3 |
| *Microhomology* | 5/47 (10.6%) | 6/53 (11.3%) | 5/47 (10.6%) |
| Average length | 2 | 2.33 ± 0.67 | 2.6 ± 0.4 |
| Range | 2 | 1–5 | 1–3 |

[a]Significant in *post hoc* analysis by unpaired *t*-test versus VprBP$^{fl/+}$-Cre$^-$.
[b]Within the D or J gene segment. All base substitutions were transition mutations.

outcome to efficient signal joint formation, and therefore concluded that the RAG1 mutants exhibit a defect in the joining step rather than the cleavage step of V(D)J recombination. However, it is difficult to ascertain from this experiment how much signal one might have expected to observe with the number of SEBs WT RAG1 would introduce in the substrate in the absence of DNA repair. As a result, it is plausible that more SEBs were introduced by WT RAG1 than the RAG1 mutants, but the WT, but not mutant, RAG1-induced SEBs were repaired efficiently. If so, both the cleavage and joining steps may be impaired by the RAG1 RING mutations, which would be consistent with what we observe.

### *VprBP regulates post-cleavage processing and repair of RAG-mediated DNA breaks*

Genetic evidence presented here suggests loss of VprBP function alters the processing and repair of RAG-mediated DNA breaks. Addition of non-templated nucleotides after hairpin resolution (N nucleotides) is attributed to the activity of members of the pol X family of polymerases, including TdT, and DNA polymerases μ (pol μ) and λ (pol λ) (Bertocci *et al*, 2006). The increased average length of inserted nucleotides observed in coding joints amplified from VprBP$^{fl/+}$-Cre$^+$ and VprBP$^{fl/fl}$-Cre$^+$ mice suggests VprBP plays a role in regulating terminal transferase activity during the repair of RAG-induced DNA breaks. This possibility gains credibility by the unexpected observation that VprBP$^{fl/+}$-Cre$^+$ and VprBP$^{fl/fl}$-Cre$^+$ mice also exhibit a higher frequency of mutations in flanking D and J segments. Filling of 3′ recessed ends or short gaps during V(D)J recombination of the heavy chain locus is attributed to pol λ activity (Bertocci *et al*, 2006). The spectrum of mutations that are introduced in VprBP$^{fl/+}$-Cre$^+$ and VprBP$^{fl/fl}$-Cre$^+$ mice D–$J_H$ coding joints includes mainly transition mutations, and single nucleotide deletions and insertions. Biochemical analysis of pol λ fidelity indicates that this enzyme has a misincorporation profile favouring transition over transversion mutations, and also exhibits a high single-base deletion rate and possesses terminal transferase activity (Fiala *et al*, 2004; Yamtich and Sweasy, 2010). The similarity between the spectrum of mutations in VprBP$^{fl/+}$-Cre$^+$ and VprBP$^{fl/fl}$-Cre$^+$ mice and the characteristics of pol λ fidelity raises the possibility that VprBP regulates pol λ activity directly or indirectly through an Ub-dependent mechanism. It is also interesting that 6/7 sequences containing transition mutations occur in coding joints that also bear N nucleotide additions. This observation suggests that N addition may be coupled to error-prone gap filling events mediated by pol λ. Similarly, the observation that the two clones containing D segment nucleotide insertions obtained from VprBP$^{fl/fl}$-Cre$^+$ mice also contain blocks of microhomology suggests such insertions are frequently associated with microhomology-directed repair.

We recognize that pol λ-deficient mice and mice expressing core RAG1 (lacking the N-terminus) in place of full-length RAG1 do not exhibit the striking developmental arrest at the pro-B-to-pre-B cell transition we observe in VprBP$^{fl/fl}$-Cre$^+$ mice (Dudley *et al*, 2003; Bertocci *et al*, 2006). This apparent discrepancy suggests that VprBP plays a role in B-cell development beyond its potential involvement in improving the efficiency and fidelity of V(D)J recombination through its association with full-length RAG1 or its regulation of pol λ activity. Since VprBP has been shown to function as a substrate receptor for other E3 Ub ligase assemblies (see below), it is possible that VprBP functions in the context of additional E3 Ub ligase complexes to target distinct substrates to regulate other pathways activated during V(D)J recombination. However, we emphasize that any potential requirement for VprBP in these other pathways can be bypassed in the B lineage by expressing functionally rearranged Ig transgenes (Figure 5).

©2012 European Molecular Biology Organization

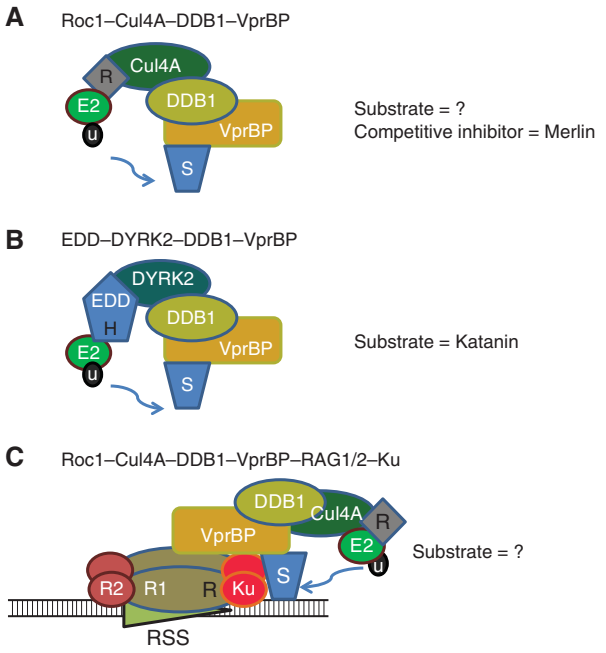


**Figure 8** VprBP and DDB1 assemble diverse E3 Ub ligase complexes. Models comparing different E3 Ub ligases containing the adaptor and substrate receptor complex VprBP/DDB1. (**A**) In the VDCR E3 ligase complex, Roc1 contains an RING (R) domain that mediates ubiquitylation and associates with DDB1 and VprBP through the scaffold protein Cul4A. (**B**) In the EDD–DYRK2–DDB1–VprBP E3 ligase complex, EDD contains an HECT domain that mediates ubiquitylation and associates with DDB1 and VprBP through DRYK2 which functions both as an adaptor subunit and as a protein kinase. (**C**) In the RAG1/2-Ku–VDCR complex, full-length RAG1 associates with RAG2 and Ku, and interacts with the VDCR complex through VprBP. The latter complex can function independently of the RAG1 RING domain to mediate ubiquitylation. Candidate substrates and inhibitors of each ligase complex are indicated where known; some remain speculative.

### *DDB1 and VprBP form diverse E3 Ub ligase assemblies involved in DNA replication, HIV replication, tumour suppression and V(D)J recombination*

VprBP was originally identified as a host interaction partner to the HIV Vpr protein (Zhang *et al*, 2001), which plays a key role in HIV infection by inducing $G_2$ cell-cycle arrest to promote HIV replication. The significance of this interaction was revealed in later studies establishing that VprBP is a member of a large family of WD40-repeat proteins that generally serve as substrate receptors for the RING-type Cul4/Roc1 E3 Ub ligase through association with the adaptor protein DDB1 (Lee and Zhou, 2007). The endogenous substrates that VprBP normally recruits to the DDB1/Cul4A/Roc1 E3 Ub ligase complex for ubiquitylation may include a tumour suppressor protein called NF2/Merlin (Huang and Chen, 2008), but Merlin may alternatively act as an inhibitor of this E3 Ub ligase complex (Li *et al*, 2010; Figure 8A). DDB1/VprBP also services the HECT-type EDD E3 Ub ligase through its association with the adaptor protein kinase DYRK2 where it reportedly promotes ubiquitylation of katanin (Maddika and Chen, 2009; Figure 8B). The finding here that full-length RAG1 associates with the VDCR complex extends the number and variety of E3 Ub ligase assemblies that use DDB1/VprBP as adaptor and substrate recognition subunits (Figure 8C). However, rather than recognizing full-length RAG1 as a substrate, the evidence presented here suggests full-length RAG1 alternatively recruits the VDCR complex to direct its E3 Ub ligase activity. In the context of the Cul4A/Roc1 and EDD E3 ligases, VprBP/DDB1 functions to regulate DNA replication and cell-cycle progression. The data presented here provide the first evidence that VprBP/DDB1 also plays a role in regulating the processing and repair of DNA breaks during V(D)J recombination. Identifying the endogenous substrates of RAG1–VDCR complex-mediated ubiquitylation will provide important mechanistic clues into how Ub modification promotes high-fidelity repair during V(D)J recombination.

## Materials and methods

#### *Mice*

All animals were housed in individually ventilated micro-isolator cages in an AALAC-accredited facility at Creighton University. All procedures were conducted in accordance with federal and institutional guidelines and approved by the University Institutional Animal Care and Use Committee. $VprBP^{fl/+}$ mice (provided by Y Xiong) and mb1-Cre mice (provided by N Gupta with permission from M Reth) have been previously described (Hobeika *et al*, 2006; McCall *et al*, 2008). IgHEL-transgenic mice (Mason *et al*, 1992) were purchased from Jackson Laboratory (Tg[IghelMD4]4Ccg).

#### *Antibodies and immunoblotting*

These reagents and procedures are described in the Supplementary data.

#### *VprBP identification*

Purified FLMR1/cMR2 was subjected to SDS–PAGE, stained with SYPRO Orange, and a gel slice containing p170 was excised from the gel and analysed by mass spectrometry following a previously published procedure (Ciborowski *et al*, 2007). VprBP was identified from multiple peptides in two independent analyses (see Figure 1B).

#### *Protein expression and purification*

Detailed procedures for the expression and purification of RAG, VprBP/DDB1 and Roc1/Cul4A proteins can be found in Supplementary data.

#### *Electrophoretic mobility shift assay*

Procedures for these assays have been described previously (Bergeron *et al*, 2006). Briefly, a radiolabelled 12RSS or 23RSS substrate was incubated with purified RAG and HMGB1 proteins (as indicated), with or without VprBP/DDB1 and/or Cul4A/Roc1 (purified from insect cells), in binding buffer at 4°C for 10 min. For supershift assays, pre-immune or anti-VprBP anti-serum (1 μl), or anti-VprBP antibody (1 μg) was added after the initial incubation period and placed on ice for an additional 5 min. The complexes were then separated on a 4% native polyacrylamide gel and analysed as previously described (Bergeron *et al*, 2006).

#### *Pull-down assays*

Purified full-length or truncated VprBP protein (2.5 μg; FL, D1, D5 and D8, respectively; see Figure 2A) and/or purified FLMR1/cMR2 (2.5 μg) were incubated in IP buffer (1% IGEPAL, 300 mM NaCl, 20 mM Tris–HCl pH 7.5, 2 mM EDTA, 50 mM sodium fluoride, 0.4 mM sodium ortho-vanadate, 0.4 mM PMSF, 1 μM pepstatin A, 5 μM leupeptin) in a final volume of (500 μl) overnight at 4°C under gentle rotation. Anti-MBP antibody (2.5 μg) was added and incubated an additional 2 h at 4°C followed by addition of protein A-agarose beads (50 μl of 50% slurry; Pierce Thermo Scientific) pre-washed three times in 1 × IP buffer containing protease inhibitors and 1 μg/μl of BSA. The mixture was incubated for 2 h at 4°C and then the beads were washed three times with 1 × IP buffer containing protease inhibitors. The beads were resuspended in 50 μl sample loading buffer and boiled, and then the supernatant was subjected to SDS–PAGE and probed by immunoblotting.


©2012 European Molecular Biology Organization

### *In-vitro ubiquitylation assays*

Following previous reports (Simkus *et al*, 2009), *in-vitro* ubiquitylation reactions (25 μl final volume) were performed in reaction buffer (40 mM Tris–HCl pH 7.5, 2 mM dithiothreitol, 5 mM $MgCl_2$, 0.1 M NaCl, 2 mM ATP), and various components were added to the reaction in different combinations as indicated: 400 μM myc–Ub, 50 nM rabbit E1 (UBE1) and 200 nM UbcH2, 3, 5a, 5b or 13 (all from Boston Biochem, Cambridge, MA), and purified cMR1/cMR2, FLMR1/cMR2, FLMR1 only or $MR1_{1-383}$ (300 ng). In some experiments, reactions were further supplemented with full-length VprBP/DDB1 (300 ng, purified from 293 cells), Cul4A/DDB1 (150 ng, purified from 293 cells), Ku70/Ku80 (350 ng, Trevigen, Gaithersburg, MD), KPNA1 (178 ng, Origene Technologies, Rockville, MD), or Histones H3.1, 3.2 or 3.3 (500 ng, New England Biolabs, Ipswich, MA). Rabbit E1 was pre-incubated with myc–Ub for 10 min at 37°C in 1 × reconjugation buffer (Boston Biochem); the remaining components were incubated on ice for 30 min. The two mixtures were then combined, and the reactions were incubated for 2 h at 37°C. The reaction mixture was then subjected to SDS–PAGE and probed by immunoblotting.

### *Flow cytometry*

Single cell suspensions prepared from bone marrow, spleen and thymi of mice with the indicated genotypes were stained with cocktails of fluorochrome-labelled antibodies or HEL as previously described (Fusby *et al*, 2010). HEL (Sigma, St Louis, MO) was conjugated to AlexaFluor 647 using a kit (Invitrogen, Carlsbad, CA). All sample data collection and cell sorting were conducted using a BD FACSAria flow cytometer. FACS purified bone marrow $B220^+CD43^+$ and $B220^+CD43^-$ populations cells were analysed for apoptosis by staining with Annexin V and propidium iodide using a commercially available kit according to the manufacturer's instructions (BD Biosciences), and evaluated for cell-cycle status by with propidium iodide according to the method of Vindelov (1977). All flow cytometric data were analysed using FloJo (TreeStar, Ashland, OR) or ModFit LT (Verity Software, Topsham, ME).

### *V(D)J recombination assays*

$D–J_H$, $V_H–DJ_H$ and $V_\kappa–J_\kappa$ rearrangements were amplified by PCR from four-fold serially diluted genomic DNA prepared from bone marrow (200, 50, 12.5 and 3 ng), and probed by Southern hybridization using procedures described previously (Schlissel and Baltimore, 1989; Schlissel *et al*, 1991). As a loading control, a CD14 fragment was amplified by PCR in parallel (Schlissel *et al*, 1993). Gel-isolated $D–J_H4$ amplicons were cloned using a TOPO-TA Cloning Kit (Invitrogen). The cloned sequences were aligned to known D and $J_H$ gene segments and the coding joints were analysed to identify junctional insertions, deletions and microhomologies (Gauss and Lieber, 1996).

### *Statistics*

Data are presented as mean values ± standard error of the means. Collected data were subjected to analysis of variance and *post hoc* testing using the PASW Statistics 19.0 software package (SPSS Inc., Chicago, IL). Differences with a *P*-value of $<0.05$ are considered statistically significant.

### *Supplementary data*

Supplementary data are available at *The EMBO Journal* Online (http://www.embojournal.org).

## Acknowledgements

We thank Colton Sutton for technical assistance; J Chen and L-J Zhao for reagents; M Reth and N Gupta for providing mb1-Cre mice; and M Lieber for helpful discussions. This work was supported by grants to PCS from the NIH (AI055599 and R56AI091748-01A1) and the LB692 Nebraska Tobacco Settlement Biomedical Research Program. Grants from the NIH/NCRR to support the Creighton University Animal Resource Facility (G20RR024001) and to acquire a Typhoon 9410 Variable Mode Imager (1S10RR027352) are also gratefully acknowledged.

*Author contributions:* MDK, KM, VLP, PR, SK, GAP, SJ, YX, PC and PCS designed the experiments; MDK, KM, VLP, PR, SK, DKA and GAP performed the experiments; MDK, KM, VLP, PR and PCS analysed the data; PCS wrote the paper.

## Conflict of interest

The authors declare that they have no conflict of interest.

## References

Ahn J, Novince Z, Concel J, Byeon CH, Makhov AM, Byeon IJ, Zhang P, Gronenborn AM (2011) The Cullin-RING E3 ubiquitin ligase CRL4-DCAF1 Complex dimerizes via a short helical region in DCAF1. *Biochemistry* **50:** 1359–1367

Bergeron S, Anderson DK, Swanson PC (2006) RAG and HMGB1 proteins: purification and biochemical analysis of recombination signal complexes. *Methods Enzymol* **408:** 511–528

Bertocci B, De Smet A, Weill JC, Reynaud CA (2006) Nonoverlapping functions of DNA polymerases mu, lambda, and terminal deoxynucleotidyltransferase during immunoglobulin V(D)J recombination *in vivo*. *Immunity* **25:** 31–41

Ciborowski P, Kadiu I, Rozek W, Smith L, Bernhardt K, Fladseth M, Ricardo-Dukelow M, Gendelman HE (2007) Investigating the human immunodeficiency virus type 1-infected monocyte-derived macrophage secretome. *Virology* **363:** 198–209

Cortes P, Ye ZS, Baltimore D (1994) RAG-1 interacts with the repeated amino acid motif of the human homologue of the yeast protein SRP1. *Proc Natl Acad Sci USA* **91:** 7633–7637

Deshaies RJ, Joazeiro CA (2009) RING domain E3 ubiquitin ligases. *Annu Rev Biochem* **78:** 399–434

Desiderio S (2010) Temporal and spatial regulatory functions of the V(D)J recombinase. *Semin Immunol* **22:** 362–369

Dudley DD, Sekiguchi J, Zhu C, Sadofsky MJ, Whitlow S, DeVido J, Monroe RJ, Bassing CH, Alt FW (2003) Impaired V(D)J recombination and lymphocyte development in core RAG1-expressing mice. *J Exp Med* **198:** 1439–1450

Fiala KA, Abdel-Gawad W, Suo Z (2004) Pre-steady-state kinetic studies of the fidelity and mechanism of polymerization catalyzed by truncated human DNA polymerase lambda. *Biochemistry* **43:** 6751–6762

Fugmann SD, Lee AI, Shockett PE, Villey IJ, Schatz DG (2000) The RAG proteins and V(D)J recombination: complexes, ends, and transposition. *Annu Rev Immunol* **18:** 495–527

Fusby JS, Kassmeier MD, Palmer VL, Perry GA, Anderson DK, Hackfort BT, Alvarez GK, Cullen DM, Akhter MP, Swanson PC (2010) Cigarette smoke-induced effects on bone marrow B-cell subsets and CD4+:CD8+ T-cell ratios are reversed by smoking cessation: influence of bone mass on immune cell response to and recovery from smoke exposure. *Inhal Toxicol* **22:** 785–796

Gama V, Yoshida T, Gomez JA, Basile DP, Mayo LD, Haas AL, Matsuyama S (2006) Involvement of the ubiquitin pathway in decreasing Ku70 levels in response to drug-induced apoptosis. *Exp Cell Res* **312:** 488–499

Gauss GH, Lieber MR (1996) Mechanistic constraints on diversity in human V(D)J recombination. *Mol Cell Biol* **16:** 258–269

Gellert M (2002) V(D)J recombination: RAG proteins, repair factors, and regulation. *Annu Rev Biochem* **71:** 101–132

Grazini U, Zanardi F, Citterio E, Casola S, Goding CR, McBlane F (2010) The RING domain of RAG1 ubiquitylates histone H3: a novel activity in chromatin-mediated regulation of V(D)J joining. *Mol Cell* **37:** 282–293

Hobeika E, Thiemann S, Storch B, Jumaa H, Nielsen PJ, Pelanda R, Reth M (2006) Testing gene function early in the B cell lineage in mb1-cre mice. *Proc Natl Acad Sci USA* **103:** 13789–13794

Huang J, Chen J (2008) VprBP targets Merlin to the Roc1-Cul4A-DDB1 E3 ligase complex for degradation. *Oncogene* **27:** 4056–4064

Jiang H, Chang FC, Ross AE, Lee J, Nakayama K, Desiderio S (2005) Ubiquitylation of RAG-2 by Skp2-SCF links destruction of the V(D)J recombinase to the cell cycle. *Mol Cell* **18:** 699–709

©2012 European Molecular Biology Organization

Jones JM, Bhattacharyya A, Simkus C, Vallieres B, Veenstra TD, Zhou M (2011) The RAG1 V(D)J recombinase/ubiquitin ligase promotes ubiquitylation of acetylated, phosphorylated histone 3.3. *Immunol Lett* **136:** 156–162

Jones JM, Gellert M (2003) Autoubiquitylation of the V(D)J recombinase protein RAG1. *Proc Natl Acad Sci USA* **100:** 15446–15451

Kirch SA, Sudarsanam P, Oettinger MA (1996) Regions of RAG1 protein critical for V(D)J recombination. *Eur J Immunol* **26:** 886–891

Lee J, Zhou P (2007) DCAFs, the missing link of the CUL4-DDB1 ubiquitin ligase. *Mol Cell* **26:** 775–780

Li W, You L, Cooper J, Schiavon G, Pepe-Caprio A, Zhou L, Ishii R, Giovannini M, Hanemann CO, Long SB, Erdjument-Bromage H, Zhou P, Tempst P, Giancotti FG (2010) Merlin/NF2 suppresses tumorigenesis by inhibiting the E3 ubiquitin ligase CRL4(DCAF1) in the nucleus. *Cell* **140:** 477–490

Lieber MR (2010) The mechanism of double-strand DNA break repair by the nonhomologous DNA end-joining pathway. *Annu Rev Biochem* **79:** 181–211

Maddika S, Chen J (2009) Protein kinase DYRK2 is a scaffold that facilitates assembly of an E3 ligase. *Nat Cell Biol* **11:** 409–419

Mason DY, Jones M, Goodnow CC (1992) Development and follicular localization of tolerant B lymphocytes in lysozyme/anti-lysozyme IgM/IgD transgenic mice. *Int Immunol* **4:** 163–175

McCall CM, Miliani de Marval PL, Chastain II PD, Jackson SC, He YJ, Kotake Y, Cook JG, Xiong Y (2008) Human immunodeficiency virus type 1 Vpr-binding protein VprBP, a WD40 protein associated with the DDB1-CUL4 E3 ubiquitin ligase, is essential for DNA replication and embryonic development. *Mol Cell Biol* **28:** 5621–5633

Mizuta R, Mizuta M, Araki S, Kitamura D (2002) RAG2 is down-regulated by cytoplasmic sequestration and ubiquitin-dependent degradation. *J Biol Chem* **277:** 41423–41427

Mombaerts P, Iacomini J, Johnson RS, Herrup K, Tonegawa S, Papaioannou VE (1992) RAG-1-deficient mice have no mature B and T lymphocytes. *Cell* **68:** 869–877

Raval P, Kriatchko AN, Kumar S, Swanson PC (2008) Evidence for Ku70/Ku80 association with full-length RAG1. *Nucleic Acids Res* **36:** 2060–2072

Rodgers KK, Bu Z, Fleming KG, Schatz DG, Engelman DM, Coleman JE (1996) A zinc-binding domain involved in the dimerization of RAG1. *J Mol Biol* **260:** 70–84

Sadofsky MJ, Hesse JE, McBlane JF, Gellert M (1993) Expression and V(D)J recombination activity of mutated RAG-1 proteins. *Nucleic Acids Res* **21:** 5644–5650

Schlissel M, Constantinescu A, Morrow T, Baxter M, Peng A (1993) Double-strand signal sequence breaks in V(D)J recombination are blunt, 5′-phosphorylated, RAG-dependent, and cell cycle regulated. *Genes Dev* **7** (12B)**:** 2520–2532

Schlissel MS, Baltimore D (1989) Activation of immunoglobulin kappa gene rearrangement correlates with induction of germline kappa gene transcription. *Cell* **58:** 1001–1007

Schlissel MS, Corcoran LM, Baltimore D (1991) Virus-transformed pre-B cells show ordered activation but not inactivation of immunoglobulin gene rearrangement and transcription. *J Exp Med* **173:** 711–720

Shinkai Y, Rathbun G, Lam KP, Oltz EM, Stewart V, Mendelsohn M, Charron J, Datta M, Young F, Stall AM, Alt FW (1992) RAG-2-deficient mice lack mature lymphocytes owing to inability to initiate V(D)J rearrangement. *Cell* **68:** 855–867

Silver DP, Spanopoulou E, Mulligan RC, Baltimore D (1993) Dispensable sequence motifs in the RAG-1 and RAG-2 genes for plasmid V(D)J recombination. *Proc Natl Acad Sci USA* **90:** 6100–6104

Simkus C, Anand P, Bhattacharyya A, Jones JM (2007) Biochemical and folding defects in a RAG1 variant associated with Omenn syndrome. *J Immunol* **179:** 8332–8340

Simkus C, Makiya M, Jones JM (2009) Karyopherin alpha 1 is a putative substrate of the RAG1 ubiquitin ligase. *Mol Immunol* **46:** 1319–1325

Spanopoulou E, Roman CA, Corcoran LM, Schlissel MS, Silver DP, Nemazee D, Nussenzweig MC, Shinton SA, Hardy RR, Baltimore D (1994) Functional immunoglobulin transgenes guide ordered B-cell differentiation in Rag-1-deficient mice. *Genes Dev* **8:** 1030–1042

Talukder SR, Dudley DD, Alt FW, Takahama Y, Akamatsu Y (2004) Increased frequency of aberrant V(D)J recombination products in core RAG-expressing mice. *Nucleic Acids Res* **32:** 4539–4549

Villa A, Sobacchi C, Notarangelo LD, Bozzi F, Abinun M, Abrahamsen TG, Arkwright PD, Baniyash M, Brooks EG, Conley ME, Cortes P, Duse M, Fasth A, Filipovich AM, Infante AJ, Jones A, Mazzolari E, Muller SM, Pasic S, Rechavi G *et al* (2001) V(D)J recombination defects in lymphocytes due to RAG mutations: severe immunodeficiency with a spectrum of clinical presentations. *Blood* **97:** 81–88

Vindelov LL (1977) Flow microfluorometric analysis of nuclear DNA in cells from solid tumors and cell suspensions. A new method for rapid isolation and straining of nuclei. *Virchows Arch B Cell Pathol* **24:** 227–242

Wang H, Zhai L, Xu J, Joo HY, Jackson S, Erdjument-Bromage H, Tempst P, Xiong Y, Zhang Y (2006) Histone H3 and H4 ubiquitylation by the CUL4-DDB-ROC1 ubiquitin ligase facilitates cellular response to DNA damage. *Mol Cell* **22:** 383–394

Wen X, Duus KM, Friedrich TD, de Noronha CM (2007) The HIV1 protein Vpr acts to promote G2 cell cycle arrest by engaging a DDB1 and Cullin4A-containing ubiquitin ligase complex using VprBP/DCAF1 as an adaptor. *J Biol Chem* **282:** 27046–27057

Yamtich J, Sweasy JB (2010) DNA polymerase family X: function, structure, and cellular roles. *Biochim Biophys Acta* **1804:** 1136–1150

Yurchenko V, Xue Z, Sadofsky M (2003) The RAG1 N-terminal domain is an E3 ubiquitin ligase. *Genes Dev* **17:** 581–585

Zhang S, Feng Y, Narayan O, Zhao LJ (2001) Cytoplasmic retention of HIV-1 regulatory protein Vpr by protein-protein interaction with a novel human cytoplasmic protein VprBP. *Gene* **263:** 131–140

 ©2012 European Molecular Biology Organization